Supplementary Materials

A novel multi-functional Zn-MOF fluorescent probe demonstrating unique sensitivity and selectivity for detection of PA and Fe^{3+} ions in water solution

Xinrui Zhuang, Xiao Zhang, Nanxi Zhang, Yan Wang, Liyan Zhao, Qingfeng Yang*

Caption of Figure

Figure S1 A view of the asymmetric unit and some symmetry-related atoms in **1**. Symmetry codes: (i) 1-x, 0.5+y, 0.5-z. (ii) 1-x, -0.5+y, 0.5-z. (iii) 1+x, 0.5-y, -0.5+z. (iv) 2-x, -0.5+y, 1.5-z. (v) 3-x, -y, 1-z.

Figure S2 The PXRD pattern of compound **1** (black: simulated from the single-crystal data, red: synthesized).

Figure S3 The IR spectral of **1**

Figure S4 Thermogravimetric analysis curve of compound **1**.

Figure S5 The PXRD of **1** immersed in acid-based solution with different pH at room temperature.

Figure S6 The PXRD of compound **1** immersed in different organic solvents at room temperature.

Figure S7 SEM image of **1** under solution treatment condition (a: blank, b: water, c: DMF, d: Toluene, e: pH = 2, f: pH = 12)

Figure S8 The solid emission spectral of ligands and **1**.

Figure S9 Emission spectra of **1** and free tpt ligand dispersed in water when excited at 282 nm, respectively.

Figure S10 The fluorescence spectral of **1** in different value of pH solution at 282 nm excitation

Figure S11 The fluorescence spectral of **1** in various organic solvents at 282 nm excitation.

Figure S12 The luminescence intensity of **1** upon incremental addition of NACs solution (5 mM) in water. (a: 2,4-DNT; b: NB; c: *p*-NT; d: *m*-DNB; e: *m*-NT; f: *o*-NT; g: *o*-Np; h: *p*-Np;).

Figure S13 Emission (at 385 nm) of compound **1** at different concentrations of PA, normalized between the minimum emission (3.3×10^{-6} M) and the maximum emission intensity (8.0×10^{-5} M). The detection limit was determined to be 2.56×10^{-6} M.

Figure S14 HOMO and LUMO energy of NACs and ligands.

Figure S15 The PXRD pattern of **1** after dealing with PA.

Figure S16 The absorbency spectral of difference NACs and emission spectral of **1**.

Figure S17 Emission spectra of **1** dispersed in different metal ions solvents when excited at 282 nm.

Figure 18. Emission (at 385 nm) of compound **1** at different concentrations of $Fe^{3+,}$ the detection limit was determined to be 4.72×10^{-6} M.

Figure 19 (a) The luminescence intensity of **1** interacting with different metal ions in water solution with and without Fe^{3+} ions. (b) The luminescence intensity of **1** upon the addition of different metal ions followed by Fe^{3+} ions.

Figure S20 The luminescence intensity of **1** and that found after three recycles; the

inserted image indicates the luminescence intensity of **1** can be recovered from Fe^{3+}–**1**.

Figure S21 The Powder X-ray diffraction patterns of **1** after cyclic sensing Fe^{3+} ions.

Figure S22 The absorption band of different metal ions solution at UV-vis light and emission spectral of **1.**

Figure S23 The PXRD pattern of **1** after dealing with Fe^{3+} ion solution.

Figure S24 The XPS of Fe^{3+}-**1** shows the typical peak of Fe^{3+} at 710 eV.

Caption of Table

Table S1 Selected bond lengths (Å) and angles (o) for **1**.

Table S2 HOMO and LUMO energies for calculated NACs at B3LYP/6-31G* level of theory.

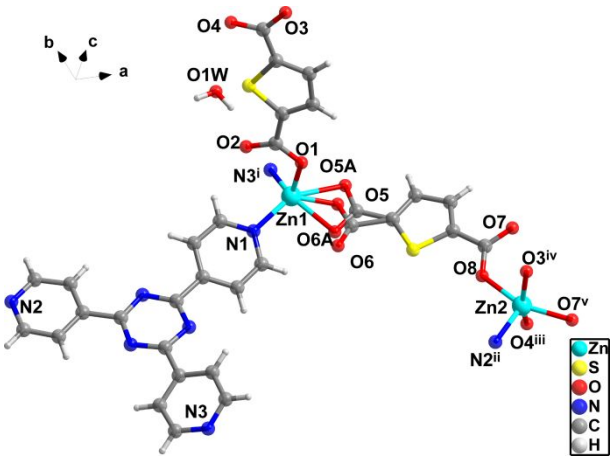

Figure S1. A view of the asymmetric unit and some symmetry-related atoms in **1**. Symmetry codes: (i) 1-x, 0.5+y, 0.5-z. (ii) 1-x, -0.5+y, 0.5-z. (iii) 1+x, 0.5-y, -0.5+z. (iv) 2-x, -0.5+y, 1.5-z. (v) 3-x, -y, 1-z.

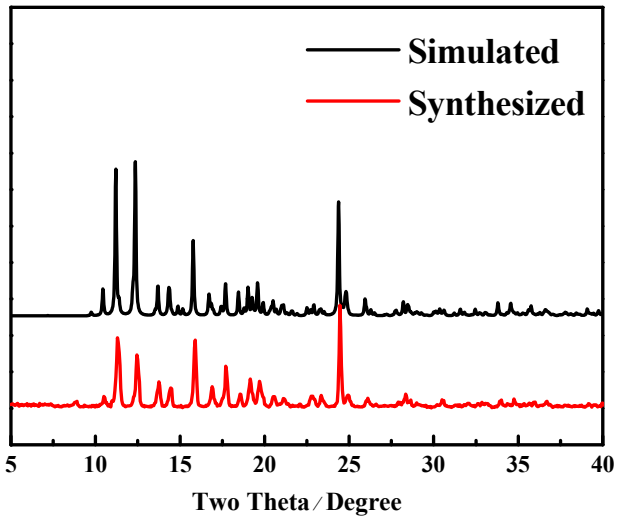

Figure S2. The PXRD pattern of compound **1** (black: simulated from the single-crystal data, red: synthesized).

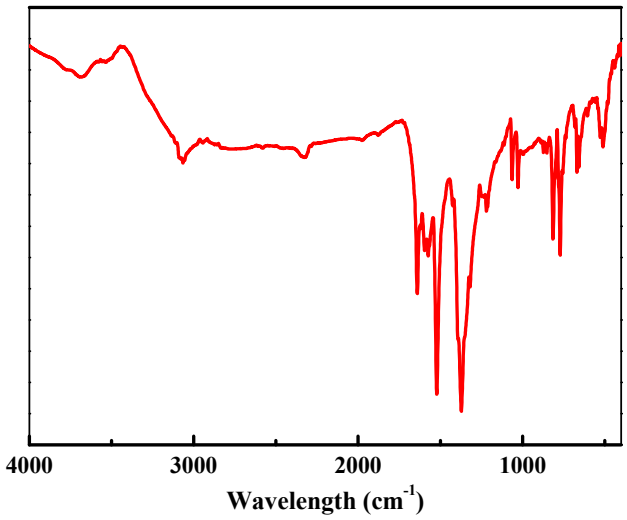

Figure 3 The IR spectral of **1**

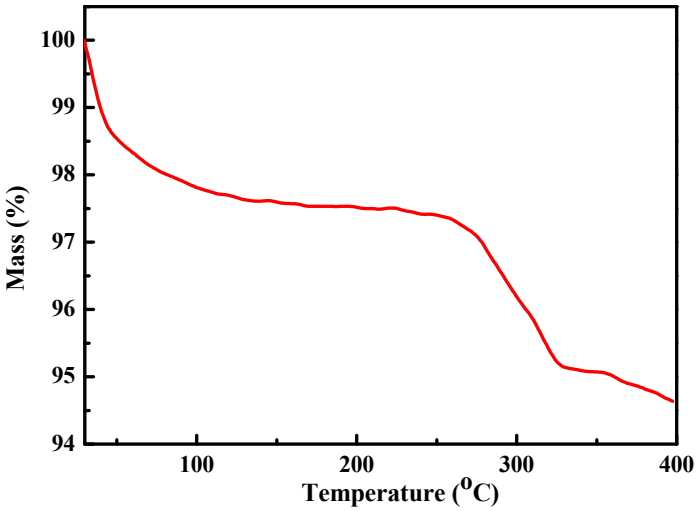

Figure S4 Thermogravimetric analysis curve of compound **1**.

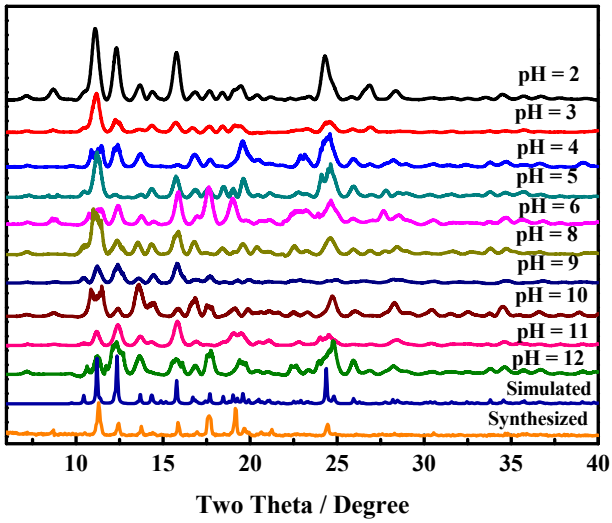

Figure S5. The PXRD of **1** immersed in acid-based solution with different pH at room temperature.

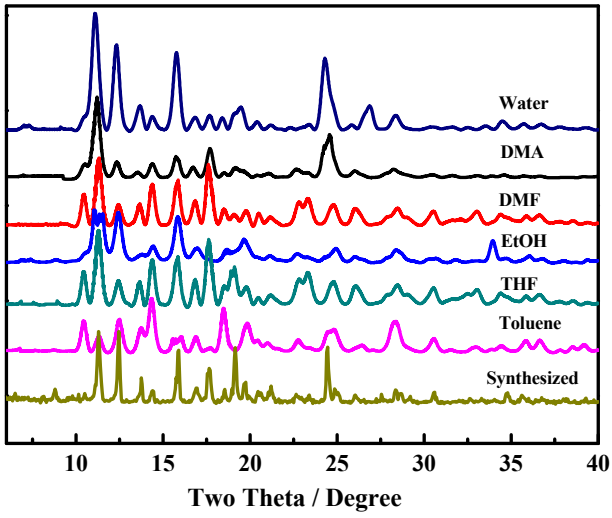

Figure S6. The PXRD of compound **1** immersed in different organic solvents at room

temperature.

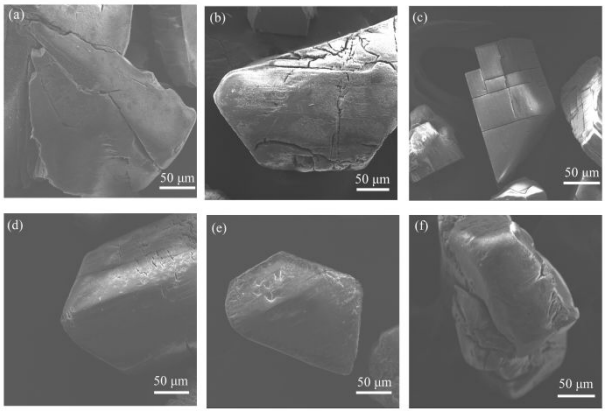

Figure S7 SEM image of **1** under solution treatment condition (a: blank sample, b: water, c: DMF, d: Toluene, e: pH = 2, f: pH = 12)

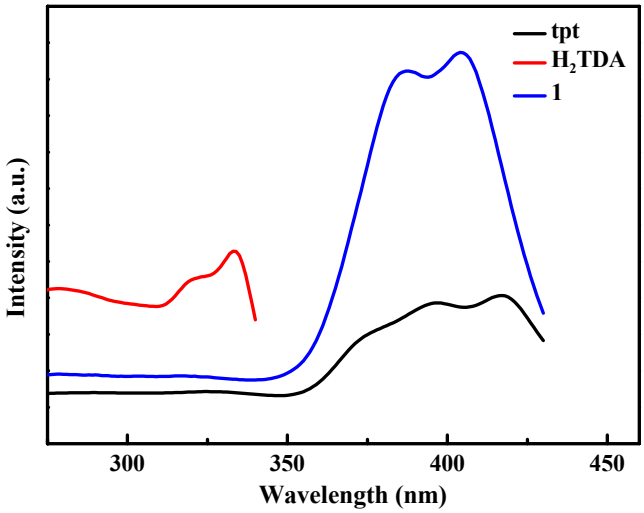

Figure S8. The solid emission spectral of ligands and **1**.

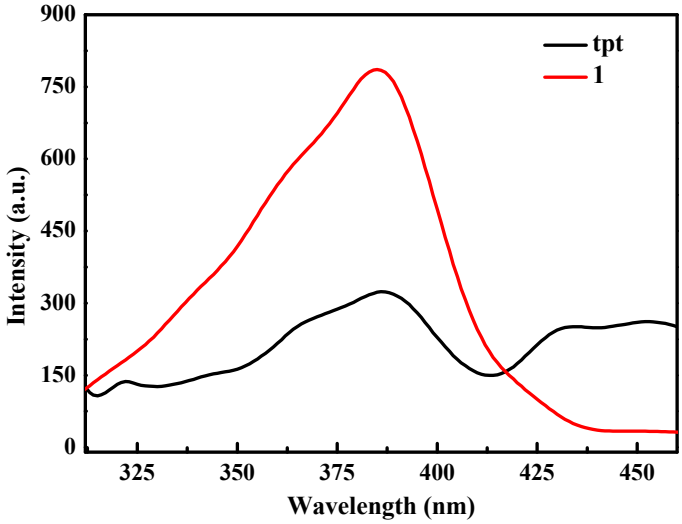

Figure S9. Emission spectra of **1** and free tpt ligand dispersed in water when excited at 282 nm, respectively.

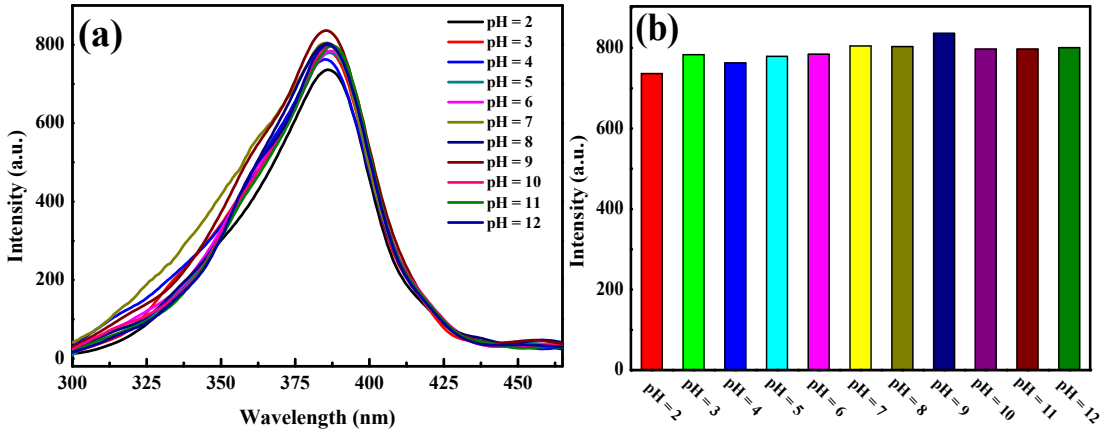

Figure S10 The fluorescence spectral of **1** in different value of pH solution at 282 nm excitation

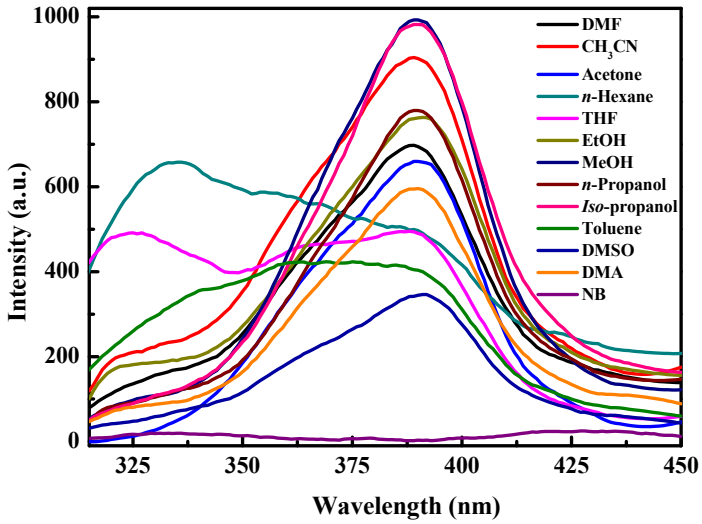

Figure S11. The fluorescence spectral of **1** in various organic solvents at 282 nm excitation.

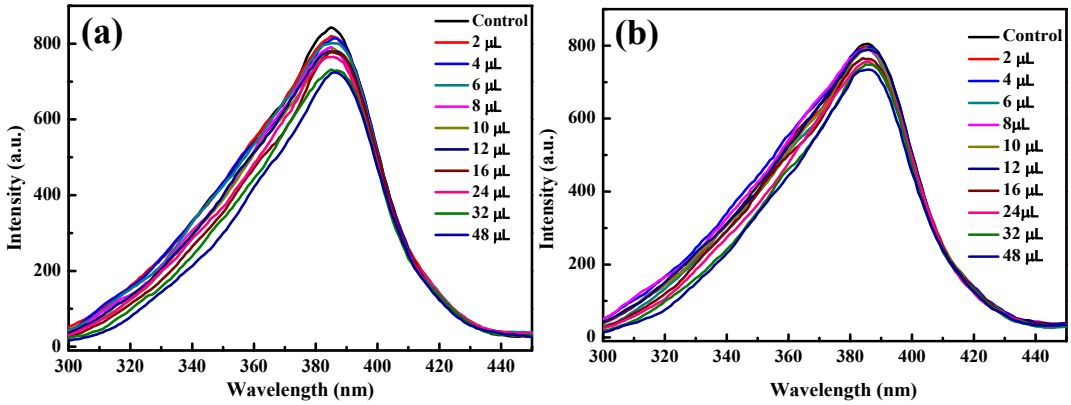

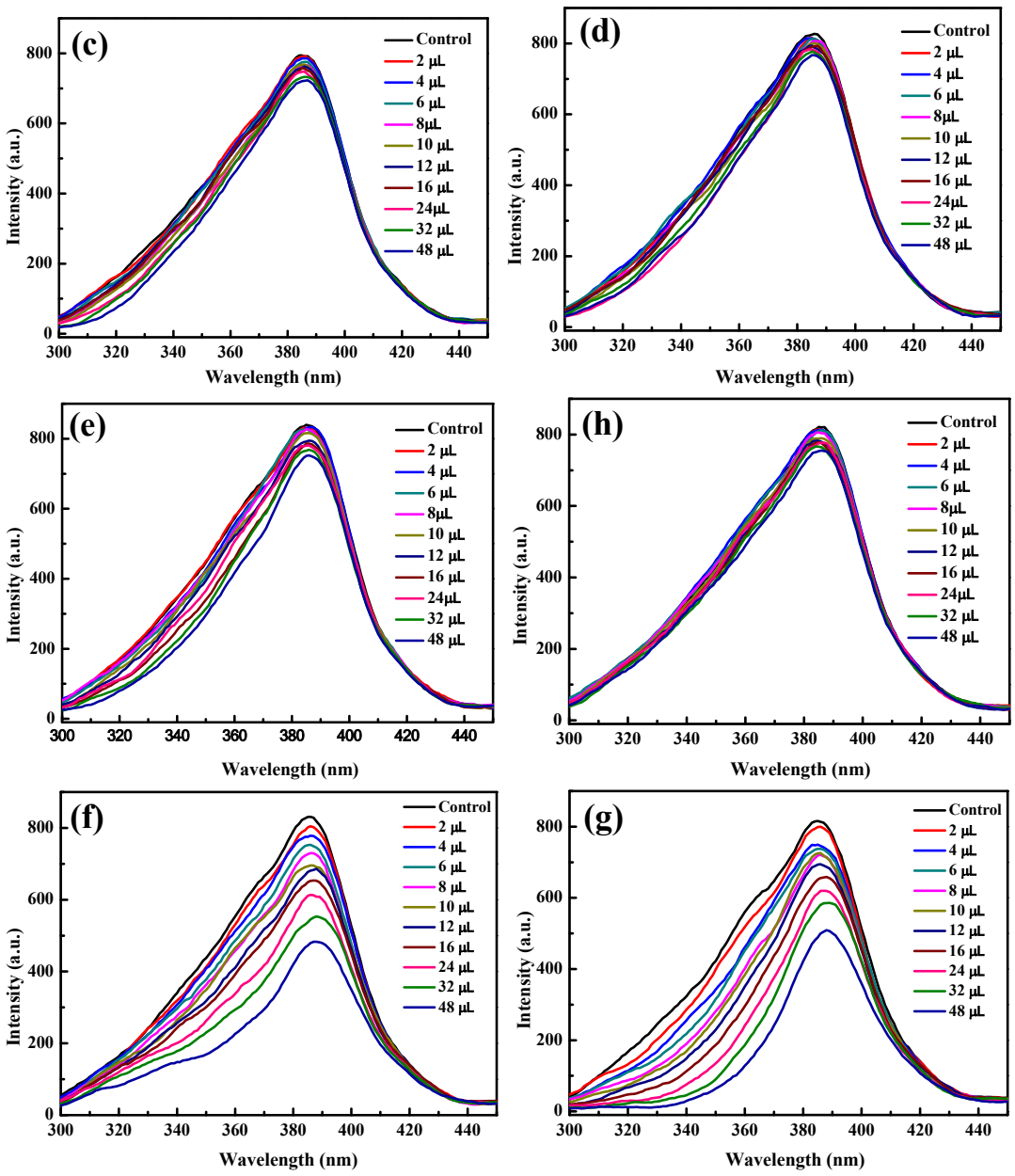

Figure S12. The luminescence intensity of **1** upon incremental addition of NACs solution (5 mM) in water. (a: 2,4-DNT; b: NB; c: *p*-NT; d: *m*-DNB; e: *m*-NT; f: *o*-NT; g: *o*-Np; h: *p*-Np).

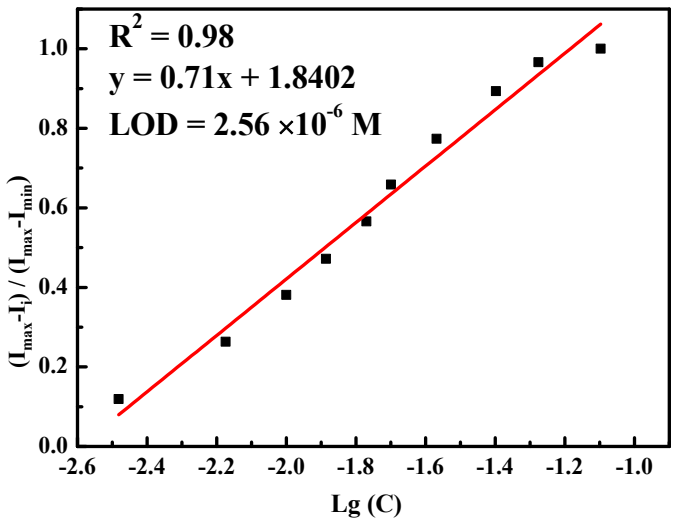

Figure S13. Emission (at 385 nm) of compound **1** at different concentrations of PA, normalized between the minimum emission (3.3×10^{-6} M) and the maximum emission intensity (8.0×10^{-5} M). The detection limit was determined to be 2.56×10^{-6} M.

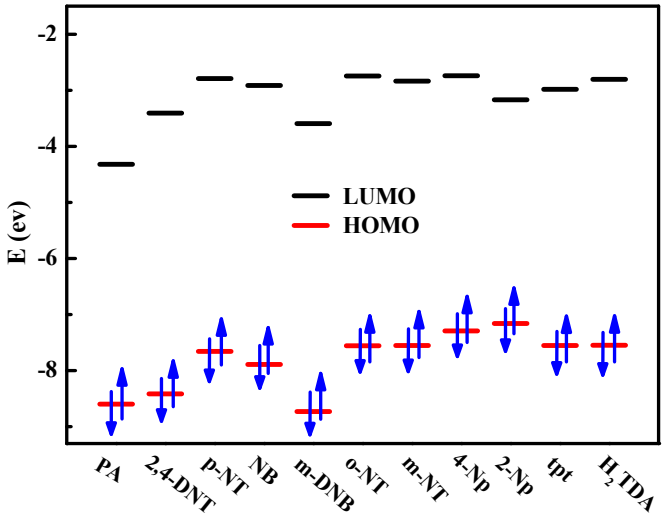

Figure S14. HOMO and LUMO energy of NACs and ligands.

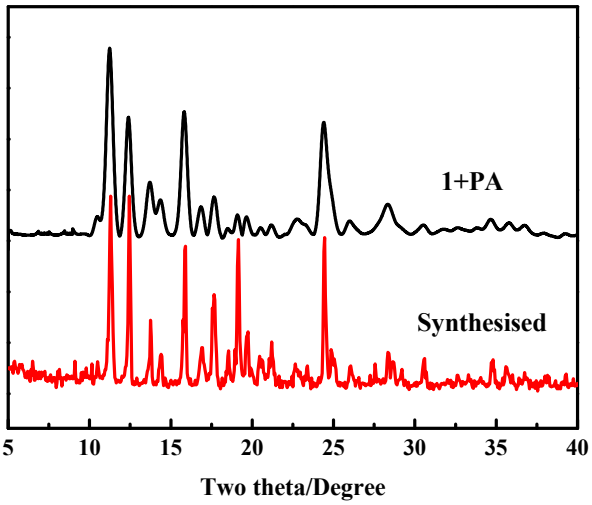

Figure S15. The PXRD pattern of **1** after dealing with PA.

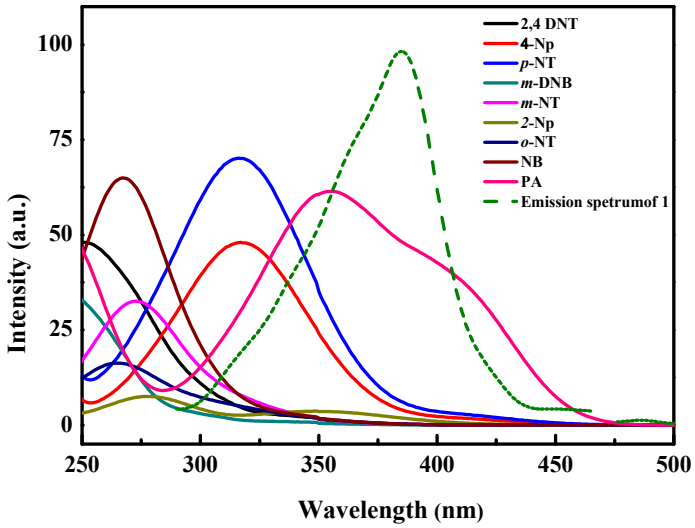

Figure S16. The absorbency spectral of difference NACs and emission spectral of **1**.

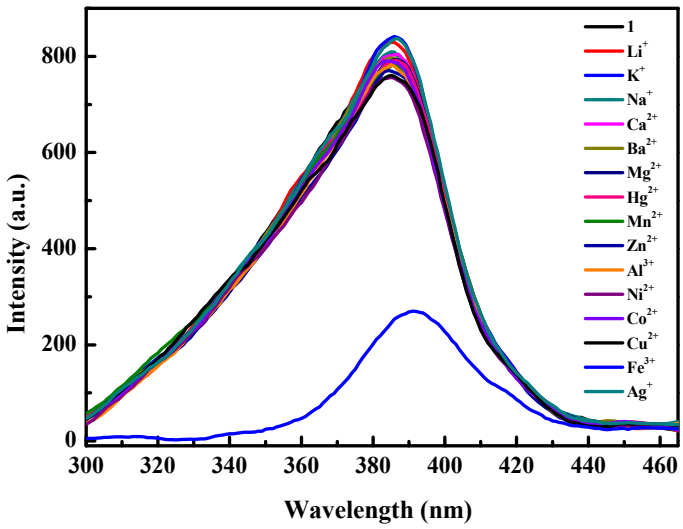

Figure S17. Emission spectra of **1** dispersed in different metal ions solvents when excited at 282 nm.

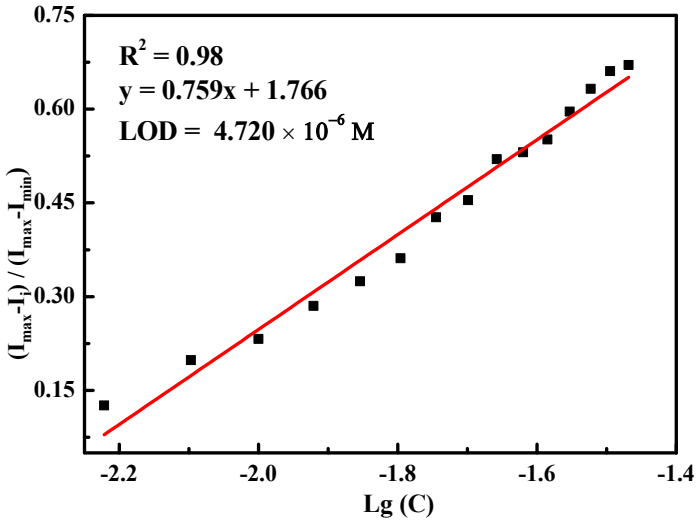

Figure 18. Emission (at 385 nm) of compound **1** at different concentrations of Fe^{3+}, the detection limit was determined to be 4.72×10^{-6} M.

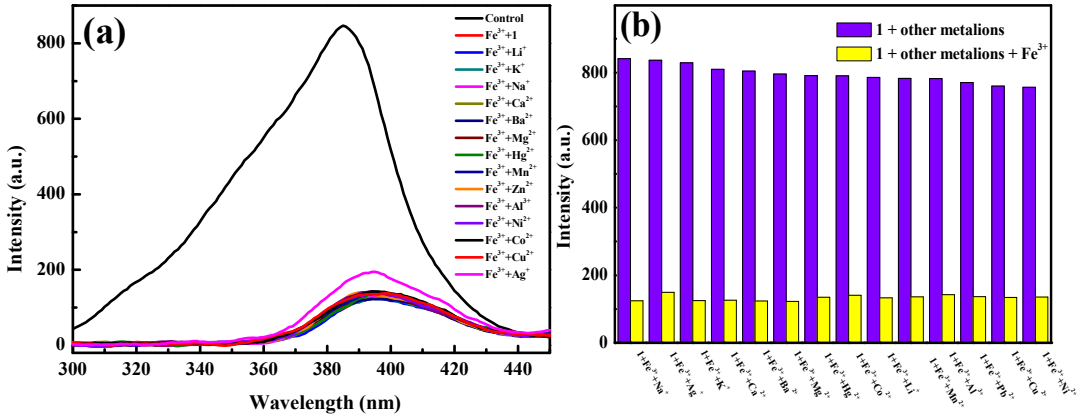

Figure 19. (a) The luminescence intensity of **1** interacting with different metal ions in water solution with and without Fe^{3+} ions. (b) The luminescence intensity of **1** upon the addition of different metal ions followed by Fe^{3+} ions.

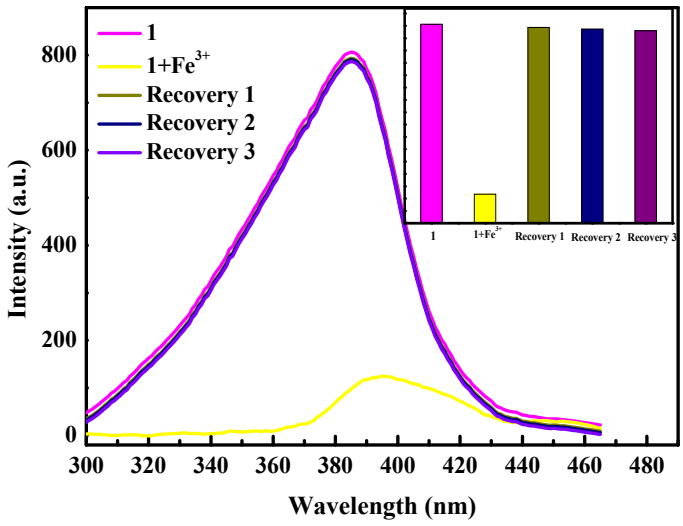

Figure S20. The luminescence intensity of **1** and that found after three recycles; the inserted image indicates the luminescence intensity of **1** can be recovered from Fe^{3+}-**1**.

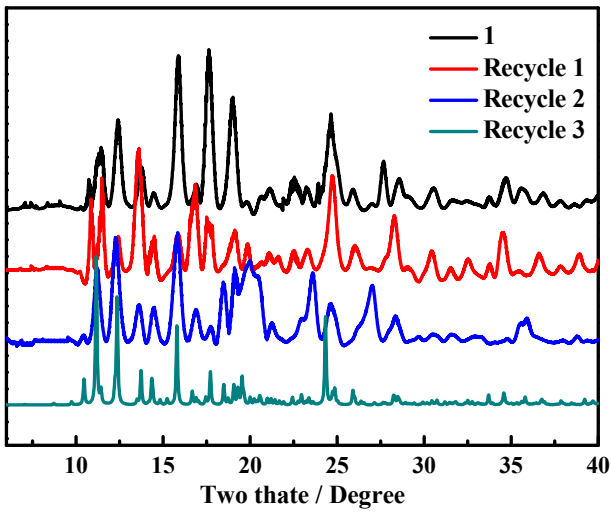

Figure S21. The powder X-ray diffraction patterns of **1** after cyclic sensing Fe^{3+} ions.

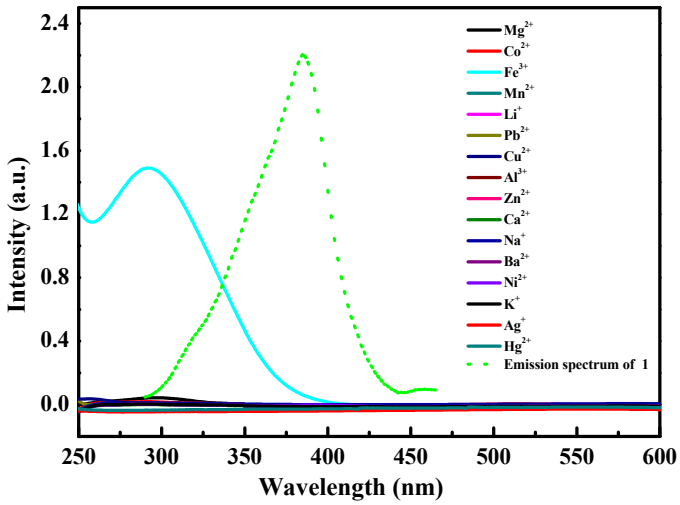

Figure S22. The absorption band of different metal ions solution at UV-vis light and emission spectral of **1**.

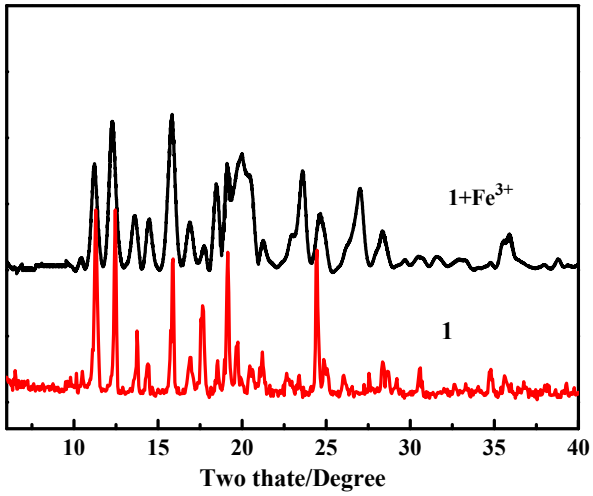

Figure S23. The PXRD pattern of **1** after dealing with Fe^{3+} ion solution.

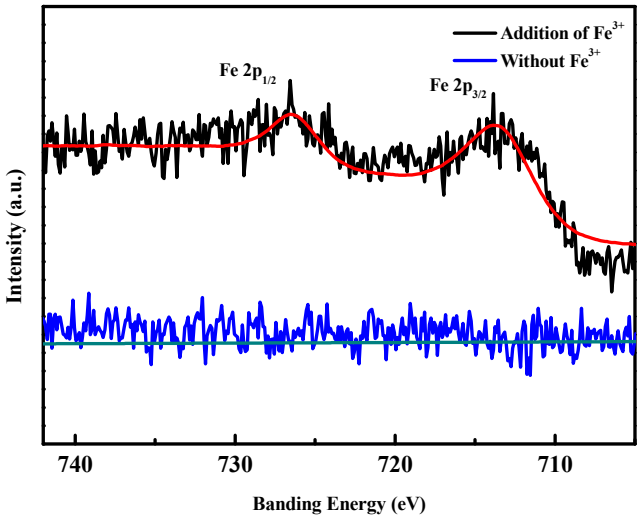

Figure S24. The XPS of Fe^{3+}-**1** shows the typical peak of Fe^{3+} at 710 eV.

Caption of Table

Table S1. Selected bond lengths (Å) and angles (o) for **1**.

Zn1-O1	1.9678(18)	Zn2-Zn2[2]	3.0129(6)
Zn1-O5	1.901(6)	Zn2-O3[3]	2.027(2)
Zn1-N1	2.0464(19)	Zn2-O7[2]	2.0388(18)
Zn1-N3[1]	2.067(2)	Zn2-O8	2.0358(19)
Zn1-O6A	2.188(11)	Zn2-N2[5]	2.0601(18)
O1-Zn1-N1	111.82 (8)	O1-Zn1-C7	93.5 (2)
O1-Zn1-O5A	88.9 (3)	O5-Zn1-N1	129.8 (3)
N1-Zn1-N3[1]	100.6 (3)	N1-Zn1-O5A	149.4 (3)
O3[2]-Zn2-O8	88.40 (9)	O4[4]-Zn2-N2[5]	108.98 (8)

[1]1−X, 1/2+Y, 1/2−Z; [2]3−X, −Y, 1−Z; [3]2−X, −1/2+Y, 3/2−Z; [4]1+X, 1/2−Y, −1/2+Z; [5]1−X, −1/2+Y, 1/2−Z

Table S2. HOMO and LUMO energies for calculated NACs at B3LYP/6-31G* level of theory.

Analytes	HOMO (ev)	LUMO (ev)	Bond gap
PA	-8.59516	-4.32093	4.27432
2,4-DNT	-8.41361	-3.40910	5.00450
p-NT	-7.65502	-2.79225	4.86279
NB	-7.88778	-2.91263	4.97515
m-DNB	-8.73052	-3.59610	5.13441
o-NT	-7.55477	-2.74677	4.80799
m-NT	-7.55031	-2.83893	4.71137
4-Np	-7.29006	-2.73967	4.55039

2-Np	-7.16037	-3.17267	3.98770
tpt	-7.55367	-2.98348	4.57019
H_2TDA	-7.54931	-2.80524	4.74407